

재활용 폴리에틸렌테레프탈레이트/폴리에틸렌 블렌드의 비등온 결정화 거동과 유변학 및 열전도 특성

Bin Yang[†], Dan Wang, Qin-Ting Chen, Jin Chen, Kang Chen, Ji-Bin Miao,
Jia-Sheng Qian, Ru Xia, and You Shi*

College of Chemistry & Chemical Engineering, Institute of High Performance Rubber Materials & Products, and
Key Laboratory of Environment-Friendly Polymeric Materials of Anhui Province, Anhui University

*College of Polymer Science & Engineering, State Key Laboratory of Polymer Materials Engineering, Sichuan University
(2019년 12월 9일 접수, 2020년 3월 4일 수정, 2020년 3월 16일 채택)

Non-isothermal Crystallization Behavior, Rheological and Thermal Conductive Properties of Recycled Polyethylene Terephthalate/Polyethylene Blends

Bin Yang[†], Dan Wang, Qin-Ting Chen, Jin Chen, Kang Chen, Ji-Bin Miao,
Jia-Sheng Qian, Ru Xia, and You Shi*

College of Chemistry & Chemical Engineering, Institute of High Performance Rubber Materials & Products, and Key Laboratory of
Environment-Friendly Polymeric Materials of Anhui Province, Anhui University, Hefei 230601, China

*College of Polymer Science & Engineering, State Key Laboratory of Polymer Materials Engineering, Sichuan University,
Chengdu 610065, Sichuan, China

(Received December 9, 2019; Revised March 4, 2020; Accepted March 16, 2020)

Abstract: In this study, we prepared series of recycled polyethylene terephthalate (RPET)/polyethylene (PE) blends using melt extrusion. The effect of RPET content on crystallization behavior and thermal conductive properties of the resultant blends were investigated using differential scanning calorimetry (DSC), dynamic mechanical thermal analysis (DMTA), etc. RPET was found to exert nucleating effect on the melt crystallization of PE. The *Agari* model presented fairly reasonable prediction of thermal conductivity as a function of RPET loading. The melt cooling process was predicted with an enthalpy transformation method (ETM), which is a well-established mean of evaluating the instantaneous heat conduction of crystalline polymers/composites, and the obtained curves were consistent with our experimental results. Besides, a four-parameter model (FPM) was adopted coupled with an *in-situ* temperature measurement in order to further disclose the solidification and crystallization kinetics of PE in the presence of RPET in the blends.

Keywords: melt blending, thermal properties, cooling behavior, recycled polyethylene terephthalate, polyethylene.

Introduction

Polyethylene (PE) is one of the widely-used thermoplastics, and can be produced into plastic tubing, film, electric cable and many other parts.¹⁻⁴ PE is relatively inexpensive, exhibits good flexibility, ease processability, and crystallinity, but possesses the disadvantages of low mechanical properties and thermal stability.⁵ Polyethylene terephthalate (PET) is known as the fourth-most-produced polymer after PE, polypropylene (PP)

and polyvinyl chloride (PVC), which is used in fibres for clothing, containers for liquids and foods, thermoforming for manufacturing, and in combination with glass fibre for engineering resins.⁶⁻¹² Products based on plastic materials will leads to environmental pollution if not properly managed (*e.g.*, littering and incinerating).^{13,14} Thus, the recycling of industrial plastics has been an ongoing practice in many industries.^{15,16} Research on the recycling and reuse of PET can be helpful to solve the environment-related problems.¹⁷

In progress of the blend modification, Kordjazi *et al.* investigated the rheological behavior of noncompatibilized and compatibilized PP/PET blends with maleic anhydride-modified styrene-ethylene-butylene-styrene polymer, and found that

[†]To whom correspondence should be addressed.
yanbin@ahu.edu.cn, ORCID[®]0000-0001-7578-4389
©2020 The Polymer Society of Korea. All rights reserved.

the storage modulus in plateau region increases by increasing the concentration of the compatibilizer.¹⁸ Shields *et al.* provided an easier insight into the mechanism of micro-/nano-fibril formation in PE/PET and PP/PET blends by studying the morphology at various stages of extrusion and drawing, and superior mechanical performance was achieved for composites containing micro-/nano-fibril structure in comparison to raw blends.¹⁹ Chen *et al.* introduced the nanoclay incorporated with ethylene-glycidyl methacrylate (E-GMA) compatibilizer into the recycled high-density polyethylene (RHDPE)/RPET blends, and found that the flexural strength and modulus, thermal stability increased gradually as the nanoclay content increased from 1% to 9%.²⁰ Wan *et al.* designed the blends of PET/PP and ternary copolymer ethylene-acrylic ester-glycidyl methacrylate (EAG) using a twin-screw extruder, and it was observed that as the EAG content increased, the loss modulus and $\tan \delta$ values of PET in the PET/PP blends remained similar to those of neat PET and the loss modulus and $\tan \delta$ values of PP in the blends decreased gradually.²¹ Raffa *et al.* reported the chemical reactions among polymer and additives showed a significant effect on the ultimate melt rheology and mechanical properties of recycled PET (RPET)/polyolefin blends.²² Chen *et al.* studied HDPE/RPET/rice husk (RH) composites through melt blending, and found that the tensile and flexural properties, water absorption and three-dimensional swelling of the resultant composites remarkably increased with increasing RH content.²³ The presence of RPET could significantly increase the thermal stability of the blend samples.^{24,25}

Present manuscript investigates the PE/RPET blends were prepared using melt mixing method to study the crystallization behavior, rheological behavior and solidification kinetics of the resultant blends *via* DSC, DMTA, rheological characterizations, *etc.* In this study, our findings showed that the presence of RPET showed nucleating effect on the crystallization of PE. The cooling process was analyzed using an enthalpy transformation method (ETM), which had proved to be an effective method for the prediction of instantaneous heat conduction of crystalline polymers (especially applicable for crystal morphological studies), *e.g.*, PE,^{26,27} PP,²⁸ PP/EPDM blend,^{29,30} *etc.* In addition, a four-parameter model (FPM) was also utilized to investigate the solidification and crystallization kinetics of the blends on the basis of the experimental results from an *in-situ* temperature measurement. Classical thermal conduction models were compared with the experimental thermal conductivity. The present work has practical significance for the further research on the “processing-structure-property” relationship of

polymer blends as well as the extension of the application fields for RPET.

Experimental

Materials. Recycled PET (RPET), with a density of 1.38 g/cm³ and melting point is 256 °C, was provided by Jinzhang (Taihu) Technology. Co., China. The melt flow index (MFI) of the RPET flakes was 27.5 g/10 min (at a load of 2.16 kg according to the GB/T 3682-2000). Polyethylene (PE) were purchased from Qilu (Shandong) Petroleum and Chemical Co., China (model: F182PC), with a MFI of 2.4 g/10 min, a solid density (ρ) was 0.920 g/cm³ and melting point is 108.4 °C.

Sample Preparation Procedures. The RPET samples were dried in a drying oven set to 50 °C for 12 h. RPET and PE were first physically blended according to a certain ratio, and then added to a twin-screw extruder (model: SHJ-20, Nanjing Jiyea Extrusion Equipment Co., China) for melt blending to produce blends (temperature process: 235, 255, 260 and 275 °C). Formula designed for this work: S0 is neat PE, the content of RPET in S1 is 22% and the content of S2 is 28%, S3 is RPET.

Dynamic Rheological Measurement. A strain-controlled rheometer (model: Bohlin Gemini-200, Malvern Instruments Ltd., U.K.) was used to characterize the dynamic rheological properties in a dynamic sweep mode. A 25.0-mm diameter parallel-plates geometry was used to prepare samples, and then disc samples of different compositions were measured at 285 °C. Prior to dynamic shear rheological measurements, a strain sweep test at a constant frequency of 1.0 Hz determined the linear visco-elastic region. After ascertaining the flow behavior, the samples subjected to dynamic oscillatory sweep from 0.01 to 100 Hz.

Differential Scanning Calorimetry (DSC) Measurements. The crystallization behaviors for the samples were studied utilizing a differential scanning calorimeter (DSC), Model: Q-2000, product of TA Instruments Inc., USA. During the measurement, each sample weighed 3~5 mg was sealed in the aluminum pans within nitrogen (N₂) atmosphere whose flow rate was 50 mL/min. The sample was heated from room temperature to 270 °C at a rate of 10 °C/min and kept at 270 °C for 4 min (to eliminated thermal history), and then cooled to room temperature at a rate of 2.5 °C/min. The crystallization behavior of the samples with a cooling rate of 5, 10, 20 °C/min was measured in this way. The crystallization behavior of the sample was analyzed by heat flow curve.

Dynamic Mechanical Thermal Analysis (DMTA). The DMTA tests for all samples were carried out on a DMA Q-800 instrument (a product of TA Instruments Inc., USA). The experiments were conducted in single/dual cantilever mode under isochronal conditions at a frequency of 1.0 Hz at a heating rate of 3.0 °C/min at controlled amplitude of 15.0 μm . The samples were pressed into a rectangular shape with dimensions about 100×10×2 mm³ at 270 °C. The storage modulus (E') and loss modulus (E'') of the samples were measured as a function of temperature. At least three samples were tested for each component, and the results were taken as the average of the test samples.

Vicat Softening Temperature. Vicat softening temperature (VST) is a temperature at which a flat-ended needle of 1 mm² circular cross section penetrates the specimen to a depth of 1.0 mm under specified conditions.³¹ In this work, the VST value was measured according to GB1634-2000 with a load of 1.02 kg at a heating rate of 120 °C/h using a XRW-300H apparatus model (product of Chengde Xinma Testing Instrument Co., Ltd.). The test specimen was a disc-like sample with a diameter of 25.0 mm and a thickness of 2.0 mm. The VST was obtained from the average value of at least 5 measurements.

Thermal Conductivity Measurement. To characterize the thermal conductivity of the samples, samples with the dimensions of 25.0 mm in diameter and 2 mm in thickness were measured by using a thermometer (model: TCI, C-THERM Inc., Canada) in an air-conditioned room (25 °C). All of the thermal measurements were performed three times and the averages were taken to calculate the thermal conductivity.

***In-situ* Temperature Measurement.** In this study, an Automatic Data Acquisition System (model: LU-R2100, Anthon Electronics Inc., China) was used to record the sample from the molten state to the cooling and solidification process in real time. The sample (ca. 4-6 g) was placed in a cylindrical metal container having a diameter of 8 mm and a height of 10 mm. The container was heated to 270 °C using an electrical hot plate (model: YOUYUE-946A, Youyue Seiko Inc., China), then held for 15 min to ensure that the sample was fully melted. A 0.5 mm diameter sensor (model: TK-247, measuring rang: 0~350 °C, Anthon Electronics Co., China) was inserted into the middle of the molten sample to quickly place the sensor-attached sample into 20 °C of circulating water until cooling solidified, the temperature corresponding to the time is displayed in the computer. The schematic of experimental set-up is illustrated in Figure 1.

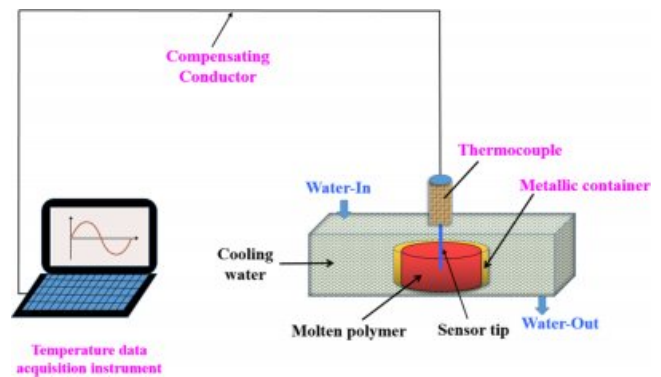


Figure 1. Schematic of experimental device for *in-situ* temperature measurement.

Results and Discussion

Dynamic Rheological Properties. Rheological characterizations are a known effective method for assessing the fluidity of material processing.³² Usually neat polymers display pseudoplastic behavior which is characteristic of an initial constant shear viscosity at low-frequency zone, and a decrease in shear viscosity with increasing frequency.³³ Figure 2 shows the frequency dependence of the complex viscosity (η^*) of all samples measured at 285 °C. With the increase of frequency, the melt viscosity decreased, and all samples displayed the shear-thinning behavior, obeying the characteristics of the pseudoplastic fluid.

The *Carreau-A* model can be adopted in this work to nonlinearly fit the rheological data of the samples.³⁴

$$\eta^* = \eta_0 \cdot [1 + (\lambda\gamma)^2]^{(n-1)/2} \quad (1)$$

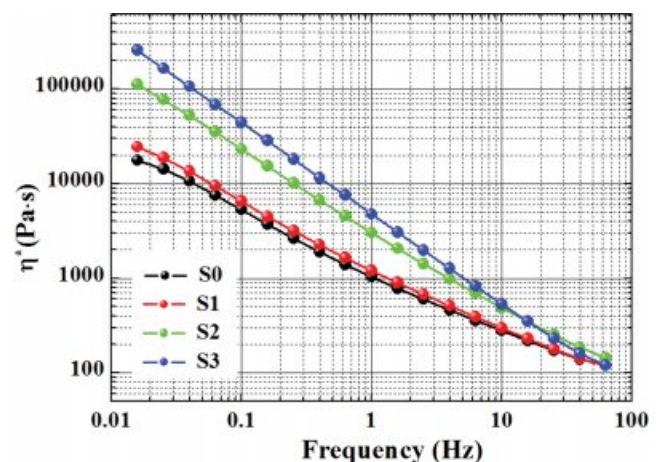


Figure 2. Complex viscosity of various samples *versus* frequency.

where η^* is the complex viscosity, η_0 the zero-shear viscosity, $\dot{\gamma}$ the shear rate, and λ the characteristic relaxation time. Here, n is the non-Newtonian exponent. Using the nonlinear fitting, all parameters were obtained and listed in Table 1. The characteristic relaxation time (λ) of the samples increased as the RPET loading increased, meaning that the disentanglement of molecular chains became more serious due to the addition of more PET macromolecular chains, whose trend is in agreement with the variation of zero-shear viscosity (η_0) as demonstrated in Table 1.

Figure 3 shows that the values of complex modulus (G^*) of the samples increased with increasing frequency. As the increase of RPET content, the G^* increased considerably, especially at the low frequency region (e.g., from 0.01 to 1 Hz), considering that G^* of PET is higher than that of PE. The G^* of the samples in the high frequency region jumped significantly with increasing frequency, which may be due to the limitation of the material's resilience after elastic deformation within high frequency region. Their G^* showed a trend of convergence at high frequencies, suggesting that the dependence of G^* on frequency became weaker in high frequency zone.

Non-isothermal Crystallization Kinetics. The non-isothermal crystallization behaviors of various samples were

Table 1. Rheological Parameters Obtained through the Carreau-A Model

Samples	η_0 (Pa·s)	λ (s)	n	R^2
S0	1.87×10^4	38.4	0.125	0.993
S1	3.07×10^4	58.2	0.144	0.998
S2	2.12×10^5	111.3	0.085	0.999
S3	9.66×10^5	236.9	0.024	0.999

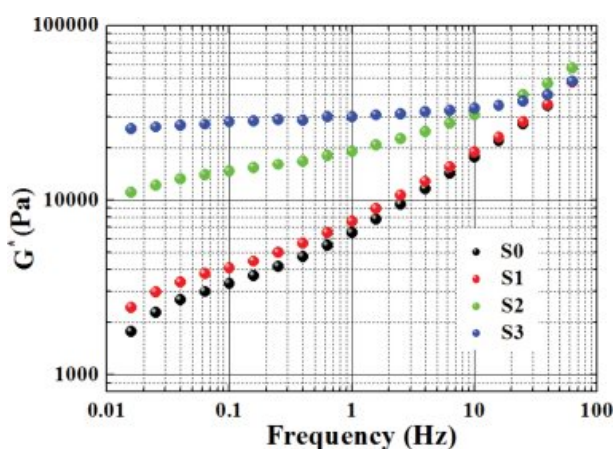


Figure 3. Complex modulus of various samples versus frequency.

examined using DSC characterization. DSC, as a multi-purpose, efficient, fast, and sensitive analytical testing method, has been widely used to study both physical changes (e.g., melting, crystallization, and crystal form transformation, etc.) and chemical changes (e.g., decomposition, degradation, polymerization, crosslinking, redox, etc.) of the substances. The absolute crystallinity (χ_c) developed during the cooling stage can be estimated using the following expression:³⁵

$$\chi_c = (\Delta H_c / \Delta H_c^0) \times 100\% \quad (2)$$

where ΔH_c is the enthalpy of melt crystallization, and ΔH_c^0 is the crystallization enthalpy of fully-crystallized PE in the cooling scans, which was taken as 288 J/g and the PET was 166 J/g.^{36,37} Table 2 presented the DSC detailed crystallization parameters at various cooling rates for various samples. With increasing cooling rate, the crystalline peak moved towards the lower temperature side, suggesting a strong supercooling was required to crystallize the melt.³⁸ Besides, the crystallization temperature curves in Table 2 all became broader with increasing cooling rate, considering the fact that imperfect polymer crystals were normally formed under rapid crystallization or at high cooling rates (cf. ΔT).³⁹ Interestingly, there is only a crystalline peak of PE in the S1 and S2 blends, while RPET has no

Table 2. Parameters of the Non-isothermal Crystallization for Various Samples

Samples	ϕ ($^{\circ}\text{C}\cdot\text{min}^{-1}$)	T_{co} ($^{\circ}\text{C}$)	T_{cp} ($^{\circ}\text{C}$)	ΔT_c ($^{\circ}\text{C}$)	χ_c (%)	$t_{1/2}$ (min)
S0	2.5	99.5	96.3	5.7	18.5	0.290
	5	98.3	94.8	6.8	21.3	0.321
	10	96.7	92.8	9.2	25.0	0.366
	20	94.5	89.5	13.1	27.0	0.452
S1	2.5	99.9	93.5	6.3	21.6	0.294
	5	98.5	90.5	8.0	24.3	0.339
	10	96.5	86.2	9.2	28.3	0.376
	20	94.5	77.9	16.6	34.7	0.462
S2	2.5	99.3	96.0	5.8	20.3	0.332
	5	97.9	94.5	7.0	23.5	0.336
	10	96.1	91.5	10.0	28.5	0.402
	20	93.9	87.7	15.1	31.1	0.459
S3	2.5	222.9	218.8	11.3	23.9	0.225
	5	219.1	214.8	12.3	25.0	0.288
	10	212.7	207.2	12.9	28.0	0.244
	20	206.3	199.4	16.1	26.9	0.478

crystalline peak. Mainly due to the slow crystalline nature of PET, and PE macromolecular chains can be inserted into the PET chain, reducing the crystallization ability of PET. With

increasing RPET content, the crystallinity of PE in the blends (*i.e.*, S1 and S2) displayed an increase trend in comparison to PE (S0), which indicated that the existence of RPET (in solid

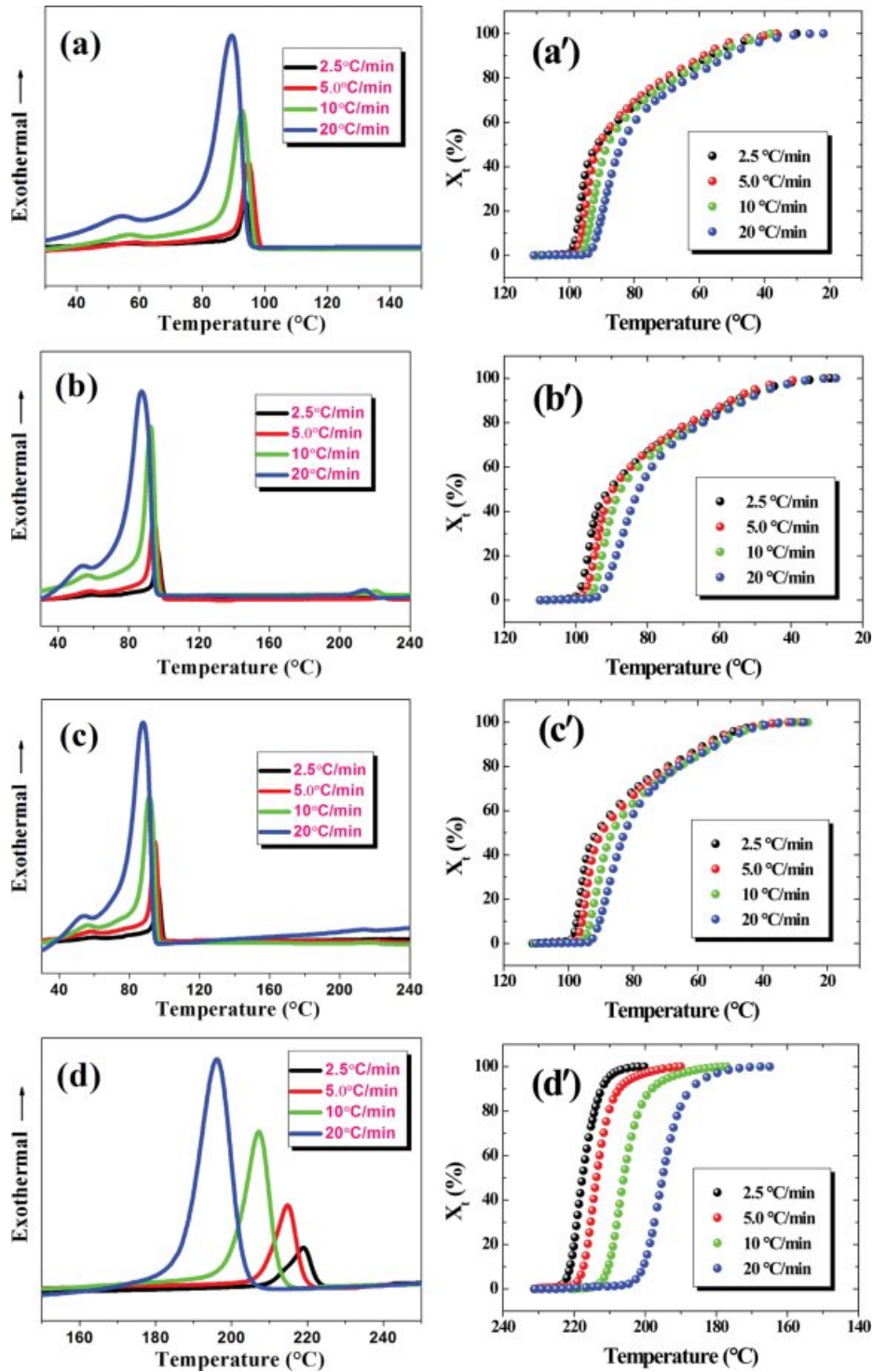


Figure 4. DSC exothermal curves of various samples measured at different cooling rates (a-d); the temperature dependence of relative crystallinity for various samples at different cooling rates (a'-d').

state during the whole crystallization temperature zone of PE) acted as nucleating agent in the blends during melt crystallization of PE.

The relative crystallinity (X_t) at time t can be expressed as a function of crystallization temperature by eq. (3):⁴⁰

$$X_t = \frac{\int_{T_0}^{T_t} \frac{dH_c}{dT_t} dT}{\int_{T_0}^{T_\infty} \frac{dH_c}{dT_t} dT} \times 100\% \quad (3)$$

where T_t is the crystallization temperature at crystallization time t and T_0 and T_∞ are the onset and end crystallization temperatures, respectively. dH_c denotes the crystallization enthalpy released during an infinitesimal temperature change at temperature T .

The molten samples were cooled for crystallization at given cooling rates, during which exothermic phenomena occurred, with the heat flow curves intuitively displaying the detailed thermal changes of the entire crystallization process. Figure 4 shows the variation of heat flow and relative crystallinity versus temperature for different samples measured at various cooling rates. All crystallinity curves of the samples displayed an “S”-like shape, including three stages of a polymer crystallization process. Specifically, the X_t value showed a significant increase after a short induction period, after which X_t gradually reached its maximum during the third crystallization. The crystallization half time ($t_{1/2}$), the time required for the polymer to reach 50% crystallinity, is an important parameter for characterizing the polymer crystallization rate. According to the results of the crystallization half time ($t_{1/2}$) which is an evaluation of the overall crystallization rate, the $t_{1/2}$ of a given sample increased with increasing cooling rate, suggesting that a rapid drop in temperature will be hinder in enhancing the crystallization rate. The addition of RPET promotes the crystallinity of the material to an extent.

As is known, the isothermal crystallization kinetics of polymers were well explained by the *Avrami* equation in the form $X_t = 1 - \exp(-K_A t^m)$, where X_t is a relative crystallization degree at the time t . K_A is a crystallization rate constant, and m is the *Avrami* exponent which is a mechanism constant depending on the types of nucleation and growth dimension.^{41,42} Table 3 presents the *Avrami* curve fitting parameters of the X_t versus crystallization time. In Table 3, the *Avrami* exponent m values of S0, S1 and S2 were 1.459~2.224, 1.402~2.254 and 1.685~2.486, respectively, indicating that the crystallization could be contributed by both one-dimensional crystal growth mecha-

Table 3. X_t Parameters Obtained Through the *Avrami* Model

Samples	ϕ (°C·min ⁻¹)	K_A	m	R^2
S0	2.5	8.15E-3	1.459	0.972
	5	2.52E-3	1.788	0.968
	10	1.41E-3	1.915	0.971
	20	3.25E-3	2.224	0.975
S1	2.5	9.83E-3	1.402	0.976
	5	2.62E-3	1.749	0.974
	10	1.64E-3	1.856	0.971
	20	2.15E-3	2.254	0.981
S2	2.5	3.33E-3	1.685	0.972
	5	2.51E-3	1.768	0.971
	10	7.21E-3	2.059	0.974
	20	1.12E-3	2.486	0.978
S3	2.5	1.31E-9	6.386	0.993
	5	5.29E-9	6.223	0.964
	10	1.18E-9	6.418	0.993
	20	6.64E-10	6.672	0.990

nisms coupled with a heterogeneous nucleation at low cooling rates (cf. 2.5 and 5 °C/min), and the crystallization of the blends occurred in two-dimensional mechanism at high cooling rates (cf. 10 and 20 °C/min). The increase in n value suggested the mode of spherulitic nucleation and the growth became more complex.

Dynamic Mechanical Thermal Analysis (DMTA) and Vicat Softening Temperature (VST) Measurement. One of the most powerful tools to investigate the viscoelastic properties of polymeric materials is dynamic mechanical thermal analysis (DMTA), which applies a very small sinusoidal strain to the sample at a constant frequency with an increasing temperature at constant rate.⁴³ Figure 5 presents the variation of storage modulus (E') as a function of testing temperature (T), respectively. The storage modulus refers to the ability of a material to store energy, which is a measure of material's stiffness.⁴⁴ In Figure 5, a severe drop of E' along the viscoelastic zone was observed until the temperature got close to 85 °C, which could be associated to the mobility of amorphous region of the material.^{43,45} As is well known, the “rubbery plateau” in the storage modulus curves represents the degree of interaction between polymeric system.⁴⁶ The sequence of E' value was as follows: $E'_{S3} > E'_{S0} > E'_{S1} > E'_{S2}$. In spite of the fact that RPET had high storage modulus, the E' of the blend hardly increased with

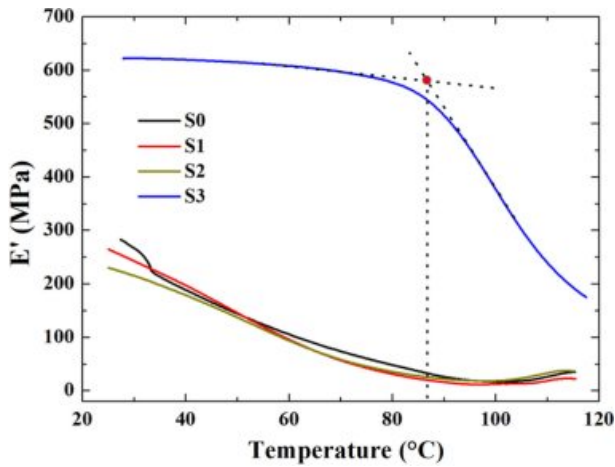


Figure 5. DMA curves of various samples.

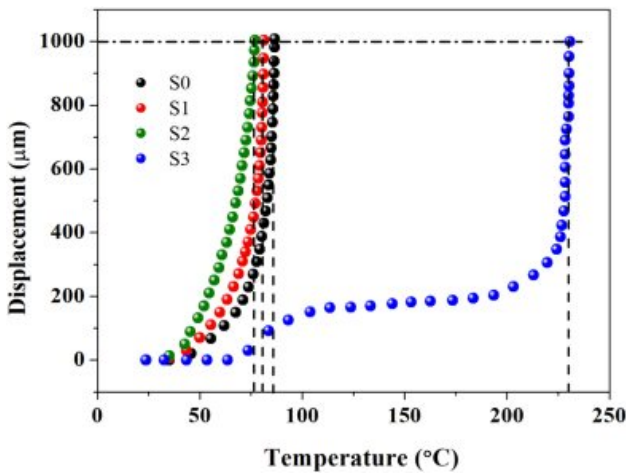


Figure 6. Curves of vicat temperature measurement.

the addition of RPET indicating that the PE/RPET presents a lower degree of interfacial interaction.^{46,47}

VST is an important parameter for the evaluation of thermal resistance of thermoplastic materials when subject to heating.⁴⁸⁻⁵⁰ The higher the VST value, the better the dimensional stability of the material upon heating, which also means, the smaller the thermal deformation, the greater the rigidity as well as the higher the modulus. According to Figure 6, the sequence of VST was as follows: $VST_{S3} > VST_{S0} > VST_{S1} > VST_{S2}$ (the VST values of S0, S1, S2 and S3 were 86.6, 81.3, 80.4 °C and 230.4 °C, respectively), indicating that S3 material has better dimensional stability when heated, and has less thermal deformation, which is well consistent with the trend of E' .

Thermal Conductive Property. Figure 7 showed the influence of PE loading on the thermal conductivity of the samples. According to the viscosity ratio, in the PE/PET blend, since the

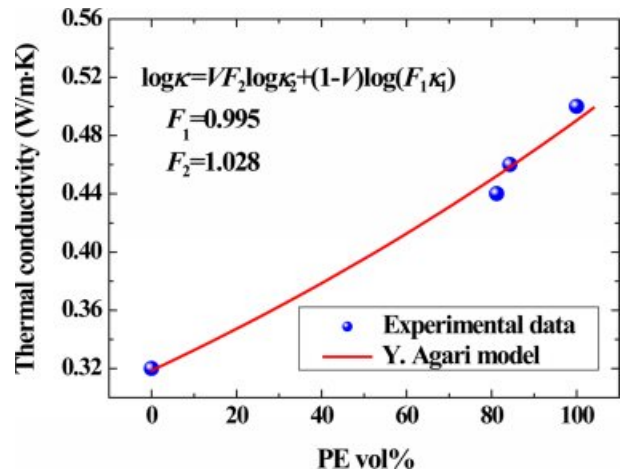


Figure 7. Correlation between thermal conductivity and PE loading as well as the fitting curve using *Agari* model.

PET content is lower than PE, the PET is dispersed as a spherical particle in the matrix of the PE, that is, “sea-island structure”.^{51,52} According to our previous research, the *Agari* model showed relatively good applicability in polymer composites, which clearly revealed formation of the thermal network structure.⁵³ The *Agari* equation can be written as follows:⁵⁴

$$\log k = VF_2 \cdot \log k_2 + (1-V) \cdot \log(F_1 k_1) \quad (4)$$

In eq. (4), k_1 , k_2 and k are the thermal conductivities of RPET, PE and their blends, respectively ($k_1=0.319$ W/m·K, $k_2=0.498$ W/m·K in this work). V is the volume content of PE here. In the *Agari* model, F_1 is usually a factor relating to the crystallinity and crystal size of polymer. Parameter F_2 varies with the dispersion state of filler (a typical range within -2~2) and is related to the ease in forming the thermal conductive chains in the matrix.^{53,54} The larger the F_2 value, the easier the formation of the thermal conductive chains (characteristic of a higher thermal conductivity). According to the calculations, F_2 is 1.028 in this study, indicating that it is easy for PE to form a thermal conductive structure in blends.

***In-situ* Melt Solidification Behavior and Application in Cooling Time Prediction.** Figure 8 demonstrated the temperature decay curves of PE, RPET and their blends, which were obtained using an *in-situ* temperature measurement technique. A cooling process of crystalline polymers basically undergoes three steps: the temperature of the melt decreases rapidly from an initial temperature to the phase-change temperature; secondly, the crystallization (accompanied with a phase change from liquid to solid simultaneously) occurs and

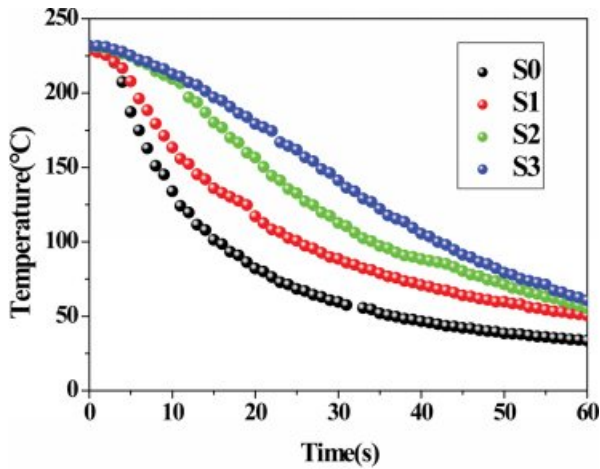


Figure 8. Temperature decay curves of various samples.

results in a slow-down in the cooling rate; finally, the cooling curves gradually become flat till the temperature gets close to the cooling medium’s temperature.

The enthalpy transformation method (ETM),⁵⁵ which was raised previously for analyzing the phase-change behavior of crystalline polymers,²⁷⁻³¹ was adopted in this work. The experimental cooling data were compared with the predicted cooling curves using ETM (as demonstrated in Figure 9), with two

dimensionless parameters (θ and τ) defined as follows:^{56,57}

$$\theta = (T - T_w) / (T_0 - T_w) \tag{5}$$

$$\tau = \alpha t / d^2 \tag{6}$$

where T , T_0 and T_w are the time-dependent melt temperature, initial melt temperature, and cooling medium temperature, respectively; θ and τ are normalized temperature and dimensionless time, respectively; α is the thermal diffusivity which is defined by $\alpha = k / (\rho \times C_p)$ with d denotes half the thickness of the molten polymer layer; k is the thermal conductivity; ρ is the density; and C_p is the heat capacity at constant pressure. The dimensionless time (τ), also known as the *Fourier* number, is a good measure of the rate of heat conduction in comparison with the rate of heat storage in a given volume element, and a small value of τ usually means rapid polymer kinetics as compared with the heat diffusion process.⁵⁸

Obviously, an agreement can reasonably be achieved from the comparison (cf. Figure 9). Overall, ETM presents relatively better prediction for neat polymer in comparison to the blends (S1 and S2), especially during the later portion of the cooling process. The cooling time (t_c) and average cooling rate (ACR)

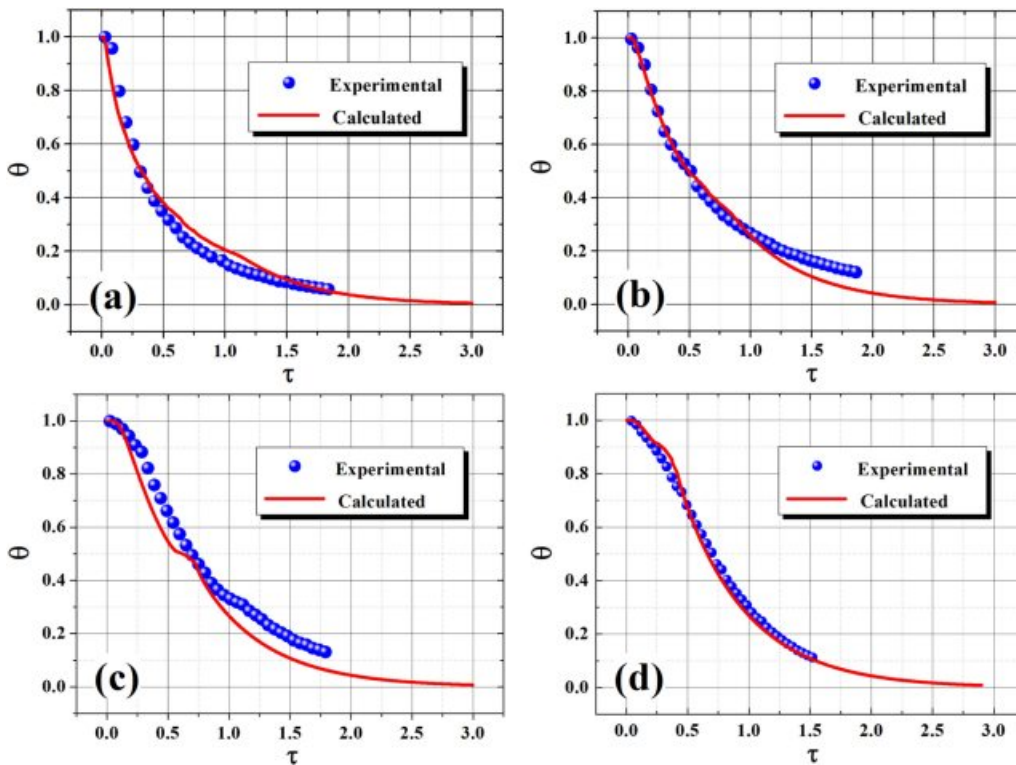


Figure 9. Plots of dimensionless temperature *versus* elapsed time.

Table 4. Cooling Parameters of Various Samples Obtained by ETM

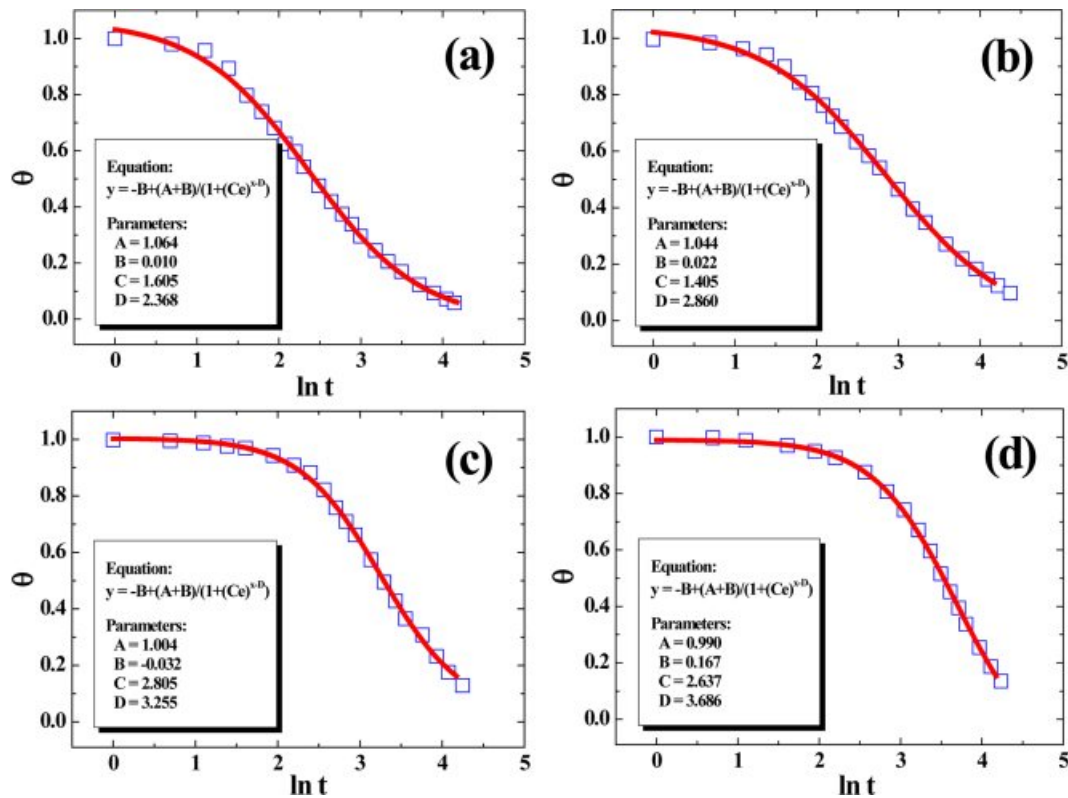
Samples	t_c (s)	τ_c/b (mm ⁻¹)	ACR (°C·s ⁻¹)
S0	44.2	0.423	4.08
S1	49.3	0.443	3.67
S2	51.6	0.447	2.95
S3	65.3	0.447	2.74

of the polymer melt can readily be evaluated, with the cooling data summarized in Table 4. As the PET content increases, the t_c value also increases (accompanied by a decreased ACR), considering the thermal conductivity of PET is lower than that of PE. Interestingly, the value of τ_c/d is found to nearly remain constant (*ca.* 0.44) regardless of the material's compositions, which can be fairly useful in forecasting the minimum cooling times (t_{cm}) for PE, PET and their blends in the plots of θ *vs.* τ during industrial processing operations (*e.g.*, injection molding, compression molding, *etc.*) when the thickness of the molded part is known. For instance, the calculated t_c value of S3 is 65.2 s in comparison to an experimental value of 68.2 s in the present work.

In our previous research, the four-parameter model (FPM) can already be used very reliably to non-linearly fit the cooling curves of various crystalline polymers (PP, PE, PVDF, *etc.*),^{59,60} which can be written as follows:

$$y = -B + (A+B)/(1 + (Ce)^{x-D}) \quad (7)$$

where $y = \theta$ and $x = \ln t$, respectively. The meanings of the parameters A , B , C and D here are as follows: A is a parameter that is primarily determined by T_0 , which is quite close to 1. B is dictated by T_w , which is close to 0. Parameter C is defined as a position-dependent coefficient of FPM; and parameter D , reflecting the time required for the temperature of polymer to fall from T_0 to the phase-change temperature range, is heavily influenced by the molecular structures of material and a smaller value of D always indicates a higher cooling rate.⁵⁹ Figure 10 presented the plots of θ *versus* $\ln t$ for the samples with cooling data fitted by FPM. It was obvious that FPM showed perfect fitting effect based upon the values of the regression coefficients R^2 , suggesting FPM can be applicable in the analysis of solidification kinetics for the PE/RPET blends. From the values of parameter D , it is obvious that D

**Figure 10.** Plots of experimental cooling data fitted using FPM, with all curves' regression coefficients (R^2) above 0.999.

decreased with the increase of PE%, suggesting that it's easier for PE to form a thermal conductive structure in blends at higher loading, which is in good agreement with our earlier discussion.

Conclusions

In this work, melt extrusion was used to prepare series of polyethylene (PE)/recycled polyethylene terephthalate (RPET) blends in an attempt to explore the effect of RPET loading on both crystallization and thermal conductive behaviors of the blends. Our findings indicate that RPET exists in an amorphous state and can act as a nucleating agent for PE without changing its crystalline form in the blend. The classical thermal conduction model by *Agari* was adopted and could present a rather reasonable prediction about the relationship between thermal conductivity and PE loading for the blends. In the study of solidification kinetic, a four-parameter model (FPM) was utilized jointly with *in-situ* temperature measurement data. In addition, cooling time (t_c) was also estimated by using an enthalpy transformation method (ETM), which had widely been reported in research on the kinetics of phase transitions analysis of crystalline polymers (HDPE, PP, PLA, *etc.*),²⁷⁻³¹ and the theoretical cooling times were in consistence with the experimental data. The present work will be practically significant for further research on the “processing-structure-property” relationship of polymer blends as well as the extension of the application fields for RPET.

Acknowledgements: The authors gratefully thank the financial support of the National Natural Science Foundation of China (Nos. 51203002, 51273001) and the “211 Project” of Anhui University. The authors are also indebted to the kind supply of materials from the Collaborative Innovation Center for Petrochemical New Materials. Dr. L. Wang from Kyoto University is appreciated for helpful advice for improvement of our work.

References

1. S. Yildirim, K. Pehlivan, A. Durmus, and K. Esmer, *Polym. Korea*, **42**, 769 (2018).
2. Y. Ahn, J. H. Jeon, J. H. Park, T. Thenepalli, J. W. Ahn, and C. Han, *Korean J. Chem. Eng.*, **33**, 3258 (2016).
3. K. Kim, D. Jung, J. Han, and J. Kim, *Polym. Korea*, **42**, 8 (2018).
4. H. Kim, Y. Yang, K. Hwang, and K. Ha, *Polym. Korea*, **41**, 1011 (2017).
5. S. C. Li and L. N. Lu, *J. Appl. Polym. Sci.*, **108**, 3559 (2008).
6. Y. S. Choi and H. Y. Jeon, *Polym. Korea*, **39**, 475 (2015).
7. Y. J. Kwak, J. H. Seo, and S. W. Lee, *Polym. Korea*, **42**, 456 (2018).
8. A. Tasic, J. D. Rusmirovic, J. Nikolic, A. Bozic, V. Pavlovic, A. D. Marinkovic, and P. S. Uskokovic, *J. Compos. Mater.*, **51**, 491 (2016).
9. S. Lee, S. Kang, and J. H. Kim, *Polym. Korea*, **41**, 287 (2017).
10. W. J. Yang and J. H. Chang, *Polym. Korea*, **39**, 746 (2015).
11. C. Fang, R. Yang, Z. S. Zhang, X. Zhou, W. Q. Lei, Y. L. Cheng, W. Zhang, and D. Wang, *RSC Adv.*, **8**, 8920 (2018).
12. S. Choi and Y. Jeong, *Polym. Korea*, **38**, 240 (2014).
13. N. S. Allen, M. Edge, M. Mohammadian, and K. Jones, *Polym. Degrad. Stabil.*, **43**, 229 (1994).
14. R. Sharma and P. P. Bansal, *J. Clean. Prod.*, **112**, 473 (2016).
15. H. P. Blom, J. W. The, and A. Rudin, *J. Appl. Polym. Sci.*, **70**, 2081 (2015).
16. M. Entezam, M. K. R. Aghjeh, and M. Ghaffari, *Radiat. Phys. Chem.*, **131**, 22 (2017).
17. M. M. Lubna, K. S. Salem, M. Sarker, and M. A. Khan, *J. Polym. Environ.*, **26**, 83 (2018).
18. Z. Kordjazi and N. G. Ebrahimi, *J. Appl. Polym. Sci.*, **116**, 441 (2010).
19. R. J. Shields, D. Bhattacharyya, and S. Fakirov, *J. Mater. Sci.*, **43**, 6758 (2008).
20. R. S. Chen, S. Ahmad, and S. Gan, *Compos. Part B-Eng.*, **131**, 91 (2017).
21. Y. W. Park, M. Park, H. Y. Kim, H. C. Kim, J. C. Lim, F. L. Jin, and S. J. Park, *Bull. Mater. Sci.*, **41**, 104 (2018).
22. P. Raffa, M. Coltelli, and V. Castelvetro, *J. Appl. Polym. Sci.*, **131**, 5829 (2014).
23. R. S. Chen, S. Ahmad, and S. Gan, *Polym. Compos.*, **39**, 2695 (2018).
24. N. R. N. Hassan, N. M. Ismail, S. Ghazali, and D. M. Nuruzzaman, *IOP Conf. Ser.: Mater. Sci. Eng.*, **342**, 012094 (2018).
25. S. Sombatdee, T. Amornsakchai, and S. Saikrasun, *Polym. Advan. Technol.*, **29**, 1123 (2018).
26. B. Yang, J. B. Miao, K. Min, R. Xia, J. S. Qian, and X. Wang, *J. Appl. Polym. Sci.*, **128**, 1922 (2013).
27. B. Yang, R. Xia, J. B. Miao, J. S. Qian, M. B. Yang, and P. Chen, *Polym. Test.*, **32**, 202 (2013).
28. B. Yang, M. Y. Ding, Y. Shi, L. Hu, R. Xia, J. B. Miao, M. Cao, J. S. Qian, P. Chen, Y. C. Zhang, and E. F. Fu, *J. Appl. Polym. Sci.*, **136**, 47390 (2018).
29. B. Yang, L. Hu, R. Xia, F. Chen, S. C. Zhao, Y. L. Deng, M. Cao, J. S. Qian, and P. Chen, *Macromol. Res.*, **24**, 74 (2016).
30. L. Hu, B. Yang, Y. L. Deng, F. X. Lu, R. Xia, Z. Z. Zheng, J. B. Miao, J. S. Qian, C. R. Zhang, P. Chen, and Y. C. Zhang, *Polym. Korea*, **41**, 569 (2017).
31. H. B. Li, Q. Li, and M. L. Yan, *Adv. Mater. Res.*, **291**, 1820 (2011).
32. Y. Shi, B. Yang, J. B. Miao, Z. Z. Zheng, J. S. Qian, L. F. Su, M.

- Cao, R. Xia, P. Chen, J. W. Liu, and G. J. Li, *Polym. Crystal.*, **2** (2019).
33. B. Zakani, M. Ansari, and D. Grecov, *Rheol. Acta*, **57**, 83 (2018).
 34. M. S. Chun and M. J. Ko, *J. Korean. Phys. Soc.*, **61**, 1108 (2012).
 35. S. Nouri, C. Dubois, and P. G. Lafleur, *Polymer*, **67**, 227 (2015).
 36. M. B. Zarandi, H. A. Bioki, Z. A. Mirbagheri, F. Tabbakh, and G. Mirjalili, *Appl. Radiat. Isotopes.*, **70**, 1 (2012).
 37. A. Granado, J. I. Eguiazábal, and J. Nazábal, *Macromol. Mater. Eng.*, **289**, 997 (2004).
 38. J. N. Martins, O. Bianchi, C. H. Wanke, C. D. Castel, and R. V. B. Oliveira, *J. Polym. Res.*, **22**, 224 (2015).
 39. C. I. Ferreira, C. D. Castel, M. A. S. Oviedo, and R. S. Mauler, *Thermochim. Acta*, **553**, 40 (2013).
 40. G. Z. Papageorgioua, D. S. Achiliasa, S. Nanakia, T. Beslikasb, and D. Bikiaris, *Thermochim. Acta*, **511**, 129 (2010).
 41. Y. P. Khanna, *Polym. Eng. Sci.*, **30**, 1615 (1990).
 42. M. Avrami, *J. Chem. Phys.*, **8**, 212 (1940).
 43. A. Elamri, A. Lallam, O. Harzallah, and L. Bencheikh, *J. Mater. Sci.*, **42**, 8271 (2007).
 44. A. Vasiljevic-Shikaleska, F. Popovska-Pavlovska, S. Cimmino, D. Duraccio, and C. Silvestre, *J. Appl. Polym. Sci.*, **118**, 1320 (2010).
 45. A. Kiziltas, D. J. Gardner, Y. Han, and H. S. Yang, *J. Therm. Anal. Calorim.*, **103**, 163 (2011).
 46. Y. H. Zhang, J. R. Choi, and S. J. Park, *Compos. Part A-Appl. S.*, **109**, 498 (2018).
 47. S. N. A. Safri, M. T. H. Sultan, M. Jawaid, and M. S. A. Majid, *Compos. Struct.*, **226**, 111308 (2019).
 48. L. F. Miranda, L. H. Silveira, L. G. Andrade e Silva, and A. H. Munhoz, Jr., *Adv. Sci. Technol.*, **71**, 138 (2010).
 49. Y. H. Liu, L. B. Bai, W. Q. Zhou, Y. W. Liu, M. Y. Tang, and K. L. Deng, *Iran. Polym. J.*, **14**, 891 (2005).
 50. Zeus Industrial Products, Inc., *Performance of High Temperature Plastics*, Technical whitepaper, 1 (2005).
 51. R. J. Shields, D. Bhattacharyya, and S. Fakirov, *Compos. Part A-Appl. S.*, **39**, 940 (2008).
 52. Z. M. Li, W. Yang, B. H. Xie, R. Huang, M. B. Yang, and J. M. Feng, *J. Macromol. Sci. B*, **43**, 519 (2004).
 53. R. Xia, M. M. Sun, B. Yang, J. S. Qian, P. Chen, M. Cao, J. B. Miao, and L. F. Su, *Polym. Korea*, **42**, 229 (2018).
 54. Y. Agari, A. Ueda, and S. Nagai, *J. Appl. Polym. Sci.*, **42**, 1665 (1991).
 55. B. Yang, Y. D. Guo, R. Xia, J. B. Miao, L. F. Su, J. S. Qian, P. Chen, and Q. L. Zhang, *J. Macromol. Sci. B*, **55**, 99 (2016).
 56. S. P. Liang, B. Yang, X. R. Fu, W. Yang, N. Sun, S. Hu, and M. B. Yang, *J. Appl. Polym. Sci.*, **117**, 729 (2010).
 57. S. Q. Deng, B. Yang, J. B. Miao, R. Xia, J. S. Qian, P. Chen, and M. B. Yang, *J. Polym. Eng.*, **32**, 355 (2012).
 58. B. Yang, X. R. Fu, W. Yang, L. Huang, M. B. Yang, and J. M. Feng, *Polym. Eng. Sci.*, **48**, 1707 (2008).
 59. B. Yang, L. Hu, G. J. Li, C. R. Zhang, J. B. Miao, R. Xia, L. F. Su, Y. L. Deng, J. S. Qian, P. Chen, and Q. L. Zhang, *Plast. Rubber. Compos.*, **46**, 200 (2017).
 60. B. Yang, M. Y. Ding, L. Hu, G. J. Li, J. B. Miao, X. Gao, X. B. Li, B. Zhang, L. F. Su, P. Chen, and J. S. Qian, *J. Macromol. Sci. B*, **58**, 42 (2019).